

NANO EXPRESS

Open Access



Enhanced Photoelectrochemical Behavior of H-TiO₂ Nanorods Hydrogenated by Controlled and Local Rapid Thermal Annealing

Xiaodan Wang^{1,2*}, Sonia Estradé³, Yuanjing Lin⁴, Feng Yu^{1,2}, Lluís Lopez-Conesa³, Hao Zhou^{1,2}, Sanjeev Kumar Gurram⁵, Francesca Peiró³, Zhiyong Fan⁴, Hao Shen^{5,6*}, Lothar Schaefer⁵, Guenter Braeuer⁵ and Andreas Waag^{1,2*}

Abstract

Recently, colored H-doped TiO₂ (H-TiO₂) has demonstrated enhanced photoelectrochemical (PEC) performance due to its unique crystalline core—disordered shell nanostructures and consequent enhanced conduction behaviors between the core-shell homo-interfaces. Although various hydrogenation approaches to obtain H-TiO₂ have been developed, such as high temperature hydrogen furnace tube annealing, high pressure hydrogen annealing, hydrogen-plasma assisted reaction, aluminum reduction and electrochemical reduction etc., there is still a lack of a hydrogenation approach in a controlled manner where all processing parameters (temperature, time and hydrogen flux) were precisely controlled in order to improve the PEC performance of H-TiO₂ and understand the physical insight of enhanced PEC performance. Here, we report for the first time a controlled and local rapid thermal annealing (RTA) approach to prepare hydrogenated core-shell H-TiO₂ nanorods grown on F:SnO₂ (FTO) substrate in order to address the degradation issue of FTO in the typical TiO₂ nanorods/FTO system observed in the conventional non-RTA treated approaches. Without the FTO degradation in the RTA approach, we systematically studied the intrinsic relationship between the annealing temperature, structural, optical, and photoelectrochemical properties in order to understand the role of the disordered shell on the improved photoelectrochemical behavior of H-TiO₂ nanorods. Our investigation shows that the improvement of PEC performance could be attributed to (i) band gap narrowing from 3.0 to 2.9 eV; (ii) improved optical absorption in the visible range induced by the three-dimensional (3D) morphology and rough surface of the disordered shell; (iii) increased proper donor density; (iv) enhanced electron-hole separation and injection efficiency due to the formation of disordered shell after hydrogenation. The RTA approach developed here can be used as a suitable hydrogenation process for TiO₂ nanorods/FTO system for important applications such as photocatalysis, hydrogen generation from water splitting and solar energy conversion.

Keywords: H-TiO₂ core-shell nanorods, Hydrogenation, Rapid thermal annealing, TEM/EELS, Optical absorption, PEC property

* Correspondence: w.xiaodan@tu-bs.de; hshen678@126.com; a.waag@tu-bs.de

¹Institute for Semiconductor Technology, TU Braunschweig, Hans-Sommer-Strasse 66, 38106 Braunschweig, Germany

⁵Fraunhofer Institute for Surface Engineering and Thin Films, Bienroder Weg 54E, 38108 Braunschweig, Germany

Full list of author information is available at the end of the article

Background

Recently, H-doped TiO_2 (H-TiO_2) has triggered broad research interest due to its enhanced photocatalytic properties. Chen et al. reported that H-TiO_2 nanoparticles were obtained by high-pressure hydrogen gas annealing. The nanoparticles contained an unique crystalline core and a disordered shell homo-interface which led to a narrowed band gap and enhanced photocatalytic behavior [1]. Wang et al. reported a new approach assisted by hydrogen plasma to synthesize H-doped black titania with core-shell nanostructures, superior to the high pressure hydrogenation process [2]. So far, the photocatalytic reports of H-TiO_2 in literature are mainly limited to nanoparticle systems [3]. There are only a few investigations about H-TiO_2 films on conductive substrates which can be used as photoanodes for *three-electrode photoelectrochemical* (PEC) studies [3]. Notably, highly oriented H-TiO_2 nanorods (NRs) and nanotubes (NTs) have been demonstrated to be highly efficient photoanodes for solar light driven water splitting [4, 5]. Such an unidirectional nanostructure decouples the processes of light absorption and charge collection, which can benefit the charge carrier separation and transport [6–8]. However, the progress of hydrogen processing methods and their influence on the structural, optical, and photoelectrochemical behaviors of H-TiO_2 is rarely reported due to lack of a practical hydrogenation method with excellent controllability on the processing parameters. Wang et al. reported a pioneer work of H-TiO_2 nanorods grown on the fluorine-doped tin oxide (F:SnO_2 ; FTO) substrate by high temperature hydrogen gas annealing in a tube furnace [4]. They studied the relation between the annealing temperature and photoelectrochemical properties. Due to the degradation issue of FTO substrate, the photocurrent density decreases at hydrogenation temperatures beyond 350°C , an intrinsic relation between the annealing temperature and photoelectrochemical properties of H-TiO_2 could not be indicated. The degradation issue of H-TiO_2 nanorods/FTO material system will restrict its applications such as photocatalysis, hydrogen generation from water splitting and solar energy conversion.

Since the hydrogen treatment can strongly influence the structural and photocatalytic properties of H-TiO_2 [9], a precise control of processing parameters (temperature, time, flux etc.) will play an important role to reproduce the core-shell structure and enhanced photocatalytic properties of H-TiO_2 in order to identify the process–structure–PEC property relationship. It is known that rapid thermal annealing (RTA) is a standard semiconductor processing technique where the processing parameters can be precisely controlled by a PC [10, 11]. It has become essential to the fabrication of advanced semiconductors such as oxidation, annealing and deposition. It can provide fast heating and cooling to process temperatures of $300\text{--}1200^\circ\text{C}$ with ramp rates typically $10\text{--}250^\circ\text{C/s}$, combined with excellent gas ambient control, allowing the creation of sophisticated multistage processes within one processing recipe. To our best knowledge, no work of H-TiO_2 nanorods hydrogenated by RTA is reported till now. In comparison to the conventional hydrogen gas annealing, RTA allows the local thermal annealing on the samples. The RTA chamber is cooled down with cycled water, only the sample and sample holder (usually Si wafer) are locally heated by a set of infrared lamps (Fig. 1). Furthermore, several sharp quartz tips are used to support the sample and Si sample holder in order to prevent the thermal loss. It is evident that RTA consumes less energy than that of conventional hydrogen gas annealing.

In this work, we report for the first time the use of the RTA method to successfully prepare H-TiO_2 nanorods grown on FTO substrate. The relationship of the processing parameters and morphology with the optical and photoelectrochemical properties is further illustrated with systematic characterization.

Methods

Growth of Ordered TiO_2 Nanorods on FTO (F:SnO_2)

Substrate

TiO_2 nanorods were directly grown on the FTO substrate via a previously reported hydrothermal method [12–14]. Typically, 0.35 ml of tetra-tert-butoxy titanate ($\text{Ti}(\text{O}^t\text{Bu})_4$) was dissolved in 30 ml of 6 M HCl, and the solution was

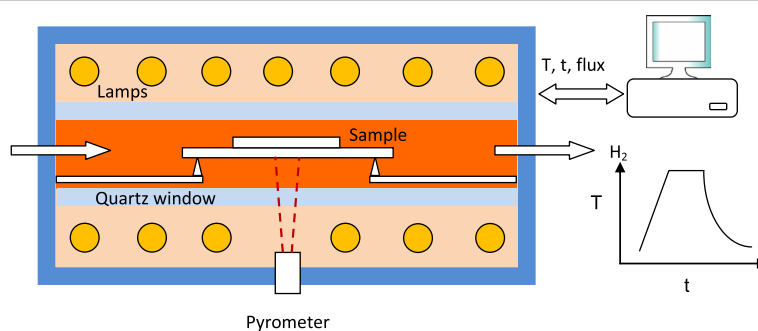


Fig. 1 Schematic of hydrogenation of TiO_2 nanorods by rapid thermal annealing (RTA) with controlled temperature recipe

transferred into a steel-lined Teflon autoclave, where a cleaned FTO substrate was placed. The autoclave was constant at 160 °C for 18 h and the coated FTO substrate was washed several times with deionized water and ethanol. To remove the chemical residues and improve the crystallinity of TiO₂ nanorods and their electric contacts with FTO glass, the samples were annealed at 550 °C for 3 h in air.

Hydrogenation of TiO₂ Nanorods by Rapid Thermal Annealing

In comparison to conventional hydrogen treatment in a tube furnace, we applied rapid thermal annealing (RTA) to make use of the controlled temperature recipes. Figure 1 shows the standard configuration of a typical rapid thermal annealing system. The samples were placed on a silicon wafer and heated by infrared lamps in hydrogen atmosphere. The temperature was measured by a pyrometer and controlled by a PID loop. All processing parameters (temperature, time, and hydrogen flux) were controlled precisely by a programmable recipe; therefore, a reproducible hydrogenation on TiO₂ nanorods could be realized. For our experiments we chose a hydrogen flux of 50 sccm, 1 bar pressure, a temperature ramping rate of 5 °C/s, and the annealing temperatures of 350, 400, and 450 °C for 1 h each.

Characterizations of the Samples

The H-TiO₂ nanorods were investigated by using a scanning electron microscope, a X-Ray diffractometer, an optical absorption spectrometer and a high resolution transmission electron microscope (HR-TEM) Jeol J2010F FEG operating at 200 kV and coupled to a Gatan GIF filter for EELS analysis.

Photoelectrochemical (PEC) Studies

A Newport solar simulator 150 W Xe lamp with AM 1.5G filter acted as a light source for the PEC test. The lamp power was adjusted using a reference silicon solar cell to obtain 100 mW/cm² (1 sun). All J-V curves were recorded with a Princeton Applied Research 2273 potentiostat using 1 M KOH as electrolyte in three-electrode configuration (Ag/AgCl in 3 M KCl as a reference electrode and platinum wire as a counter electrode). The IPCE were performed based on Oriel QE-PV-SI (Newport Corporation) and electrochemical workstation (CHI660E, China). The M-S measurements were performed on the electrochemical workstation (Gamry, USA).

Results and Discussion

To study the possible change of morphology and crystal phase of H-TiO₂ nanorods, scanning electron microscopy (SEM) images and X-ray diffraction (XRD) spectra were collected. Figure 2b shows the in-plane and cross-

sectional SEM images of H-TiO₂ nanorods treated at 400 °C. No changes of morphology and alignment are observed before and after RTA treatment. The nanorods show a good vertical alignment and similar length indicating high quality of H-TiO₂ nanorod arrays. Figure 2c shows the XRD patterns of H-TiO₂ nanorods treated at 350, 400, and 450 °C. The (101) and (002) diffraction peaks confirmed the good alignment of TiO₂ nanorods on the FTO substrate [12–14]. After the hydrogenation, the intensities of (101) and (002) diffraction decrease indicating the generation of disordered shell around the TiO₂ nanorods. In comparison to the (101) peak, the intensity of (002) decreases more when the annealing temperature increases. It indicates that the tips of TiO₂ nanorods are treated stronger than the sidewalls near to the FTO substrate.

The microstructures of single H-TiO₂ nanorod and the outmost disordered shell were further investigated by high-resolution transmission electron microscopy (TEM). Figure 3 shows the TEM images of as-prepared and H-treated TiO₂ nanorods. The as-prepared TiO₂ nanorods are confirmed to be single crystalline (Figs. 3a–c) whereas the H-treated TiO₂ nanorods show a single crystalline core and disordered shell heterostructure [15]. The amorphous shell of the sample treated at 400 °C (Figs. 3d–f) is ca. 4 nm whereas the shell of the sample-treated at 450 °C (Figs. 3g–i) becomes thicker and defective.

The optical absorption spectra of as-prepared TiO₂ and H-TiO₂ were recorded in order to study the modified optical absorption behavior of H-TiO₂. Additional file 1: Figure S1a shows the small red-shift of band edge and gradual increase of visible absorption with increasing the annealing temperature. The Tauc plot (Additional file 1: Figure S1b) shows the band gap narrowing from 3.0 to 2.9 eV. The disordered shell contains a lot of oxygen vacancies and hydrogen atoms fill up partially in positions of oxygen vacancies which is assumed to result in the slight deformation of the rutile lattice cells and the band structure [16]. It is noted that the as-prepared TiO₂ nanorods show the increased visible absorption in the range of 400–850 nm (Additional file 1: Figure S1a). This is due to the multi-step scattering of photons between the 3D nanorods. The visible absorption in the range of 400–850 nm of H-TiO₂ nanorods increases further with increasing hydrogenation temperature. It could be attributed to the rough and porous shells and the altered absorption properties of the disordered shell of H-TiO₂ nanorods to trap more visible photons.

To evaluate the photoelectrochemical behavior of H-TiO₂ nanorods, J-V and IPCE measurements were performed in a three-electrode electrochemical system. Figure 4 shows that H-TiO₂ nanorods exhibit a significant change in PEC performance with a maximum photocurrent density after hydrogen treatment at 400 °C. The photocurrent

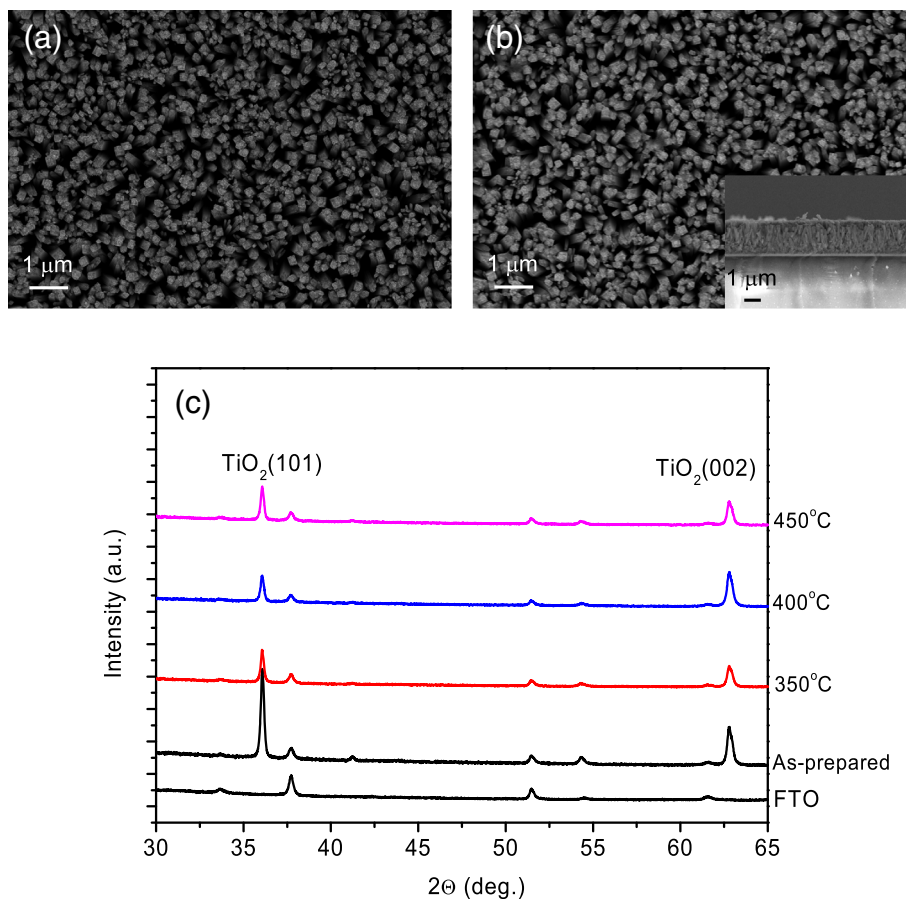


Fig. 2 SEM images of (a) as-prepared TiO₂ and (b) H-TiO₂ nanorods treated at 400 °C. c XRD patterns of H-TiO₂ nanorods treated at different temperatures

density of H-TiO₂ treated at 400 °C saturates at a lower potential of -0.4 V vs Ag/AgCl whereas the density of as-prepared TiO₂ saturates at -0.2 V vs Ag/AgCl. The photocurrent density of H-TiO₂ treated at 400 °C reaches ca. 3.7 mA/cm² at 0.23 V vs Ag/AgCl, which is more than four times larger than that of the as-prepared TiO₂. The corresponding photoconversion efficiency is shown in Additional file 1: Figure S2.

To clarify the influence of annealing temperature on the photoactivity, IPCE measurements were performed on the as-prepared and H-treated samples at 0.23 V vs Ag/AgCl (Fig. 5). IPCE can be expressed by the equation (eq. 1):

$$IPCE = \frac{1240J_p}{\lambda J_\lambda} \times 100\% \quad (1)$$

where J_p is the measured photocurrent density at a specific wavelength, λ is the wavelength of incident light, and J_λ is the measured irradiance at a specific

wavelength. Figure 5 shows that the as-prepared TiO₂ exhibits a maximum of about 45% IPCE at a wavelength of around 390 nm, consistent with literature data of rutile TiO₂ nanorods. It is interesting to note that the IPCE of H-TiO₂ shows an overall enhancement in the 300–600 nm range. The IPCE curves of H-TiO₂ have three interesting features: (i) large increase of IPCE in the UV range from 300 to 400 nm; (ii) The band edge is red-shifted from 410 to 425 nm which is also observed in optical absorption spectra (Additional file 1: Figure S1); (iii) The IPCE of H-TiO₂ samples show enhancement of IPCE in the visible (400–600 nm) range, in comparison to that of as-prepared samples. The 400 °C treated sample shows the best IPCE values in the range of 300–600 nm.

The influence of annealing temperature on H-TiO₂ was further studied by Mott-Schottky (M-S) plots (Fig. 6). It is expected that the slope of H-TiO₂ decreases with increasing annealing temperature indicating the increased donor density and conductivity according to the Mott-Schottky equation (eq. 2)

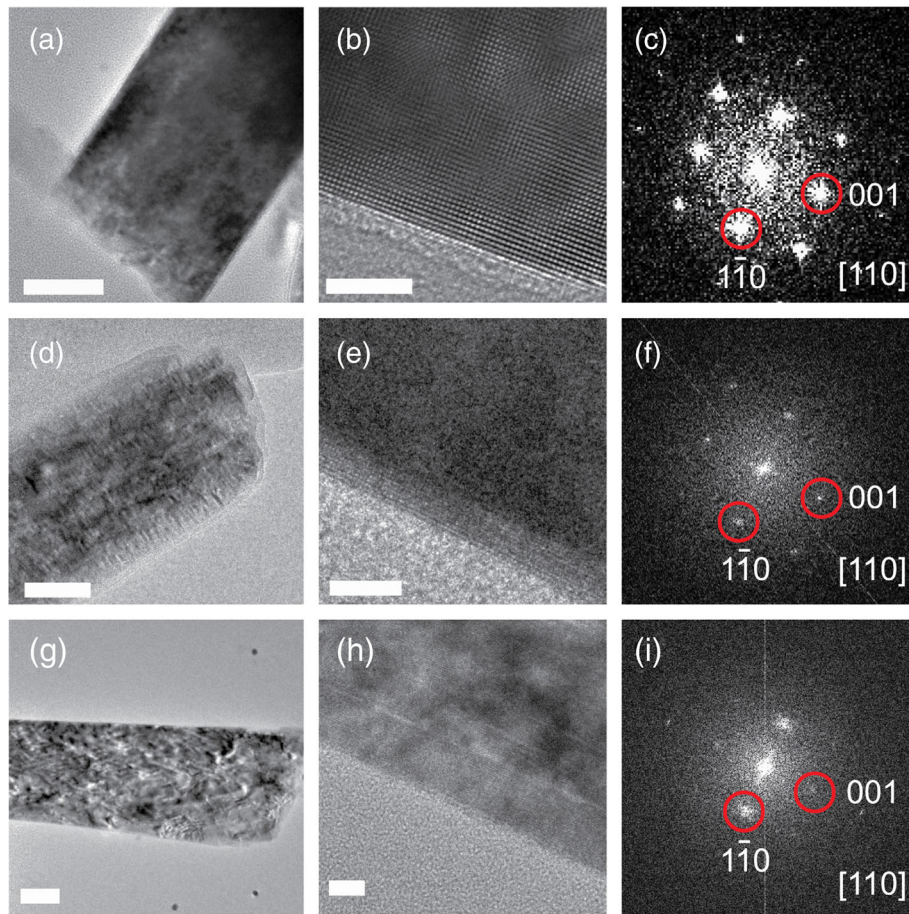


Fig. 3 TEM, HR-TEM and FFT images of (a–c) as-prepared TiO₂ nanorods and H-TiO₂ treated at 400 °C (d–f) and 450 °C (g–i). The scale bar of Figs. 3a, d, g is 50 nm whereas the scale bar of Figs. 3b, e, h is 5 nm

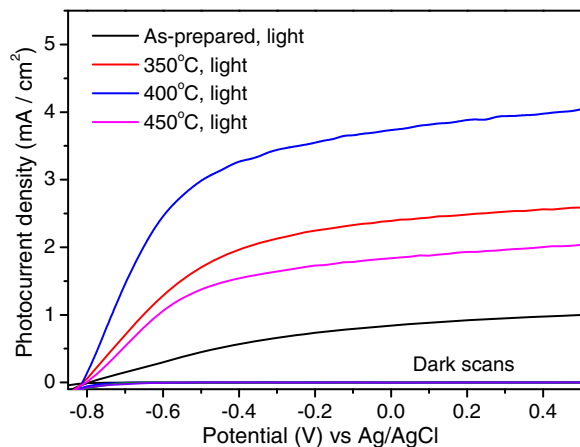


Fig. 4 J-V curves of pristine TiO₂ and H-TiO₂ nanorods in 1 M KOH solution in the dark and under solar illumination (light)

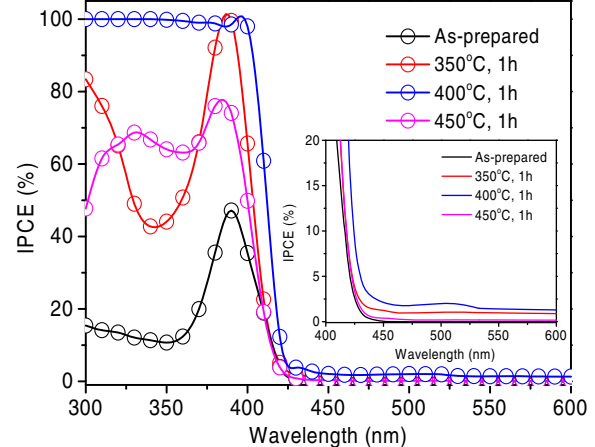


Fig. 5 IPCE spectra of pristine TiO₂ and H-TiO₂ nanorods measured at the bias potential 0.23 V vs. Ag/AgCl

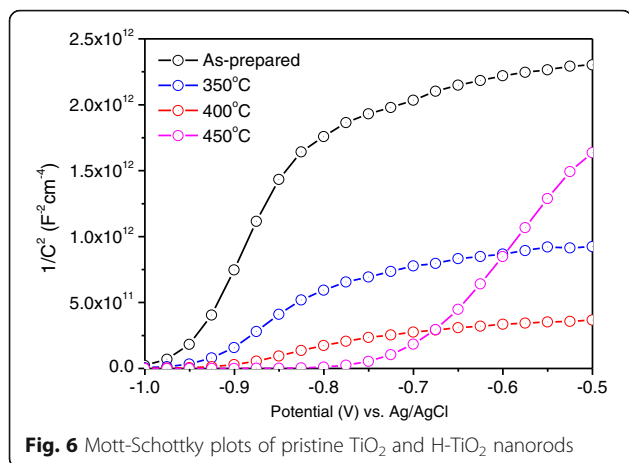


Fig. 6 Mott-Schottky plots of pristine TiO₂ and H-TiO₂ nanorods

$$N_d = \left(\frac{2}{e_0 \epsilon_0 \epsilon_r} \right) \left[\frac{d(1/C^2)}{dV} \right]^{-1} \quad (2)$$

where N_d is the donor density, e_0 is the electron charge, ϵ_r is the dielectric constant of TiO₂ nanorods, ϵ_0 is the permittivity of vacuum, and V is the applied bias voltage. The calculated donor densities of H-TiO₂ are $5.2 \pm 0.1 \times 10^{17} \text{ cm}^{-3}$ (350 °C), $2.1 \pm 0.1 \times 10^{18} \text{ cm}^{-3}$ (400 °C) and $3.0 \pm 0.2 \times 10^{17} \text{ cm}^{-3}$ (450 °C) which are higher than that of the as-prepared TiO₂ ($1.5 \pm 0.1 \times 10^{17} \text{ cm}^{-3}$) [17]. The 450 °C treated sample shows abnormal M-S plot which may be attributed to the more defective structures which is observed in the TEM image (Fig. 3g). Additionally, the flat band potentials (V_{fb}) of as-prepared and H-TiO₂ were determined by the extrapolation of straight line to the abscissa in the Mott-Schottky plots (Fig. 6). The V_{fb} of H-TiO₂ treated at 350 °C is similar to that of as-prepared TiO₂, however, the V_{fb} was observed to decrease from -0.95 V (pristine TiO₂) to -0.97 V for the H-TiO₂ treated at 400 °C. The negative shift of V_{fb} after RTA hydrogenation at 400 °C could be attributed to the substantially increased donor density (Additional file 1: Table S1), which could consequently shift the Fermi level (E_F) of H-TiO₂ towards to the conduction band (E_c). The V_{fb} was observed to increase from -0.95 V (pristine TiO₂) to -0.71 V for the H-TiO₂ treated at 450 °C. It could be due to the inhomogeneous defective structure (Fig. 3g) and decreased donor density (Additional file 1: Table S1).

To study the possible degradation of the FTO electrode in the RTA process, the sheet resistance of FTO treated at 350, 400, and 450 °C was measured by the four-probe method. In comparison to untreated FTO (~18.13 Ohm/sheet), the sheet resistances of the FTO after RTA treatment are unchanged (Fig. 7). Wang et al. reported the investigation of H-TiO₂ nanorods by hydrogen gas annealing in a furnace tube and observed the degradation of the FTO layer when the temperature was

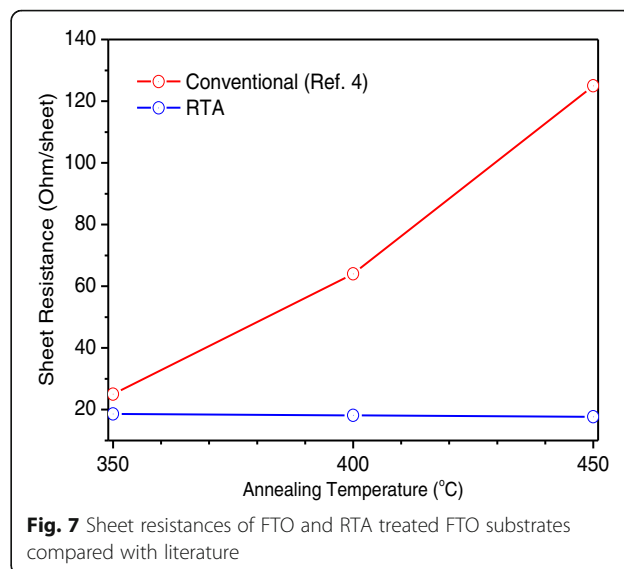


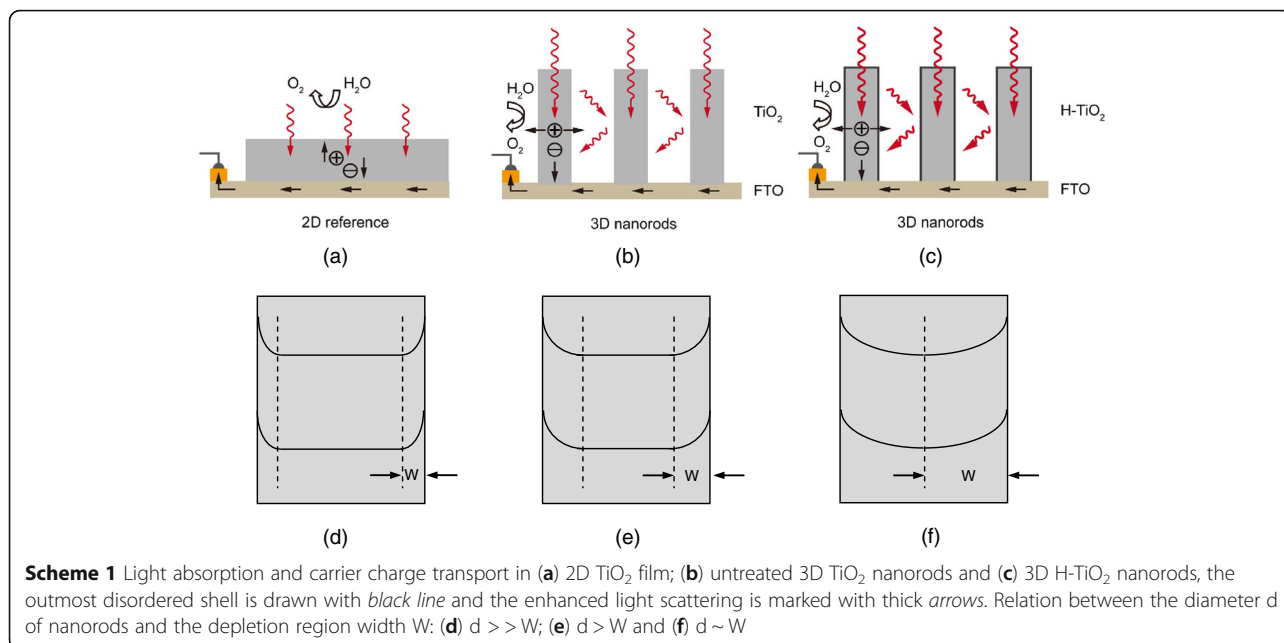
Fig. 7 Sheet resistances of FTO and RTA treated FTO substrates compared with literature

higher than 350 °C (Fig. 7) [4]. In that study, it was difficult to study the effect of temperature-dependent hydrogen gas treatment due to the degradation issue of FTO layer. As no FTO degradation is observed in RTA process, the relation between RTA processing temperature, H-TiO₂ structure and its properties can be discussed here in order to understand the mechanism of enhanced PEC performance. Our results could be related to the following factors:

(i) 3D morphology of H-TiO₂ nanorods

In comparison to 2D films, 3D nanorods with subwavelength-scale induce the light-trapping effect [18–21]. When the light is incident on the surface of 3D nanorods, the photons will be reflected back and forth between the nanoscale gaps resulting in an increase of light absorption (Scheme 1). Higher optical absorption and lower reflection are the important factors in achieving higher photocurrent density. Cho et al. compared the current density with the best data of 2D and 3D TiO₂ from literature [22]. It is evident that 3D TiO₂ can achieve the photocurrent density 1 mA/cm^2 , three times higher than that of 2D TiO₂ (ca. 0.3 mA/cm^2) because 3D TiO₂ can simultaneously offer larger surface area with electrolyte, higher optical absorption and shorter diffusion path length of holes from bulk via the surface into the electrolyte than those of 2D TiO₂.

Furthermore, the optical spectra of H-TiO₂ (Additional file 1: Figure S1) show a band gap narrowing and an enhanced visible absorption after the RTA hydrogenation. Cho et al. prepared branched TiO₂ nanorods and co-doped C, W-TiO₂ to achieve an enhancement of the visible optical absorption and PEC performance [22, 23].



It is evident that the 3D surface of TiO₂ nanorods will be used not only for morphology change, but also for the change of optical absorption via chemical doping or hydrogenation in our work.

(ii) The role of disordered shell (TiO_{2-x}H_y)

The HR-TEM results show that the thickness of disordered shell increases with increased annealing temperature which is rarely reported in literature (Fig. 3). The EELS line-scan (Additional file 1: Figure S3) shows the O/Ti ratios across a single nanorod of as-prepared TiO₂ and H-TiO₂ treated at 400 °C, respectively. The O/Ti ratio of as-prepared TiO₂ remains constant whereas the O/Ti ratio of H-TiO₂ treated at 400 °C decreases gradually in the ca. 4 nm range of disordered shell. Recently Lü et al. prepared TiO₂ homo-junction films consisting of an oxygen-deficient amorphous layer on top of a highly crystalline layer in order to simulate the crystalline core-disordered shell configuration of black TiO₂ nanoparticles [24]. They observed that metallic conduction was achieved at the crystalline–amorphous homo-interface via electronic interface reconstruction, which may be the main reason for the enhanced electron transport of black H-TiO₂. Since the composition of the disordered shell is important to understand the crystalline core-disordered shell homo-interface, detailed structural analysis will be performed in future studies.

We compared the IPCE data with literature in order to understand the improved PEC performance. Wang et al. reported nearly 100% IPCE above band-gap and less than 0.5% IPCE in the visible light range for the best samples treated at 350 °C [4]. Yang et al. reported ca.

80% IPCE above band-gap and less than 1.5% IPCE in the visible range [25]. Our IPCE spectrum of H-TiO₂ treated at 400 °C shows nearly 100% IPCE in the UV range and ca. 2.5% IPCE in the visible range, additionally the band edge is red-shifted indicating a bandgap narrowing from 3.0 to 2.9 eV. This results in higher photocurrent density during operation, in comparison to literature.

The influence of the disordered shell on the PEC performance could be: (i) *efficient electron–hole separation*: Fabrega et al. studied the relationship between the donor density (N_d) and the corresponding depletion region width (W) [17]. If the donor density is too high, the depletion region width is more localized nearby the nanorods surface which results in lower electron–hole separation efficiency (Scheme 1d). Therefore the control and optimization of donor density by hydrogenation will play a key role to achieve high PEC performance. Additional file 1: Table S1 shows the N_d values as a function of RTA annealing temperatures. It is evident that the donor density initially increases with increasing annealing temperature up to 400 °C. The depletion region width of 400 °C treated sample is ca. 78 nm which is close to the diameter of TiO₂ nanorods. It means that the H-TiO₂ nanorods are fully depleted and the electron–hole separation takes place in the whole nanorods (Scheme 1f). For higher temperatures the increasing disorder leads to a decrease in the PEC properties indicating an optimum treatment temperature at 400 °C. (ii) *efficient hole injection*: Pesci et al. performed transient absorption (TA) to study the lifetime of photo-generated holes [26]. Effective suppression of microsecond to seconds charge carrier recombination could be the key factor to improve the photoelectrochemical activity of H-TiO₂.

Table 1 RTA vs. conventional hydrogen gas annealing

Hydrogenation methods	Conventional hydrogen gas annealing	RTA
Chamber	Small sized samples Hot wall High energy consumption	Small and large scaled samples (<4") Cool wall Low energy consumption → Local heating and soft treatment
Ramping/cooling time	~ Several hours	~ Several seconds or minutes
Holding time	~0.5-1 h	~1 h
Sheet resistance of FTO	Increased with increased annealing temperatures	Unchanged with increased annealing temperatures
Achieved photocurrent density (mA/cm ²) at 0.23 V versus Ag/AgCl	2.5 (Ref.4) 2.9 (Ref.15)	3.7 (This work)

In comparison to the diameter of TiO₂ nanorods, the less than 5 nm thick disordered shell is more like a surface cocatalyst [27, 28] which can (i) remove the surface electron trapping states; and (ii) promote hole injection into the electrolyte.

(iii) Hydrogenation issues of H-TiO₂ nanorods/FTO system

In recent years, one-dimensional (1D) TiO₂ nanorod arrays on FTO substrate received broad interest due to their utilization in important applications such as photocatalysis, hydrogen generation from water splitting and solar energy conversion [3]. It is clear that TiO₂ nanorods/FTO system is not suitable for high temperature hydrogenation. The decreased conductivity of the FTO substrate is due to the formation of Sn metal upon reductive high temperature hydrogenation, the photocurrent of H-TiO₂ nanorod photoanode is limited by the decreased FTO conductivity [4]. Our investigation shows that RTA approach is better than the conventional hydrogen gas annealing and could be a suitable solution for the hydrogenation of TiO₂ nanorods / FTO system. Here, the H-TiO₂ nanorods/FTO system without *FTO degradation* by RTA treatment could provide better performance in the above-mentioned applications [3].

The physical insight for the decreased PEC performance of H-TiO₂ upon high temperature hydrogenation is not entirely understood. Leshuk et al. proposed that high temperature hydrogenation could be counterproductive to improving the photocatalytic activity of TiO₂ because of its propensity to form bulk vacancy defects [29]. In comparison to TEM image of 400 °C treated sample, the H-TiO₂ treated at 450 °C shows inhomogeneous contrast and more defective structures (Fig. 3g) indicating *strong structure destruction of TiO₂* during the hydrogenation process at higher temperature. It is clear that a controlled and suitable hydrogenation process is required for the development of H-TiO₂ systems because their PEC properties are strongly determined by the art of treatment.

Conclusions

In summary, we presented a controlled and local RTA hydrogenation method to treat TiO₂ rutile nanorods and studied the effects of annealing temperature on the structural, optical and PEC properties of H-TiO₂ nanorods. Our investigation shows that the improvement of PEC performance could be attributed to (i) band gap narrowing from 3.0 to 2.9 eV; (ii) improved optical absorption in the visible range induced by the three-dimensional (3D) morphology and rough surface of the disordered shell; (iii) increased proper donor density; (iv) enhanced electron–hole separation and injection efficiency due to the formation of disordered shell after hydrogenation. As there is an optimum of the PEC properties with respect to the hydrogenation process, the RTA method with its precise control over the processing parameters could be used as one of the standard hydrogenation processes for large-scale industrial applications. The features of RTA and conventional hydrogen gas annealing are summarized in Table 1. It indicates that RTA is more efficient than the conventional hydrogen gas annealing.

Additional file

Additional file 1: Table S1. Donor density (N_d), flat band potential (V_{fb}) and depletion region width (W) of pristine TiO₂ and H-TiO₂ nanorods calculated from the Mott-Schottky plots. **Figure S1.** (a) Optical absorption spectra of pristine TiO₂ and H-TiO₂ nanorods. (b) Tauc plots of optical absorption curves for pristine TiO₂ and H-TiO₂ nanorods. **Figure S2.** Photoconversion efficiency of pristine TiO₂ and H-TiO₂ nanorods. **Figure S3.** The O/Ti ratio distribution along the nanorod diameter (a) pristine TiO₂ and (b) H-TiO₂ nanorods treated at 400 °C. The O/Ti ratio is estimated using EELS spectra taken from a cross-line shown in the TEM image. (DOCX 930 kb)

Abbreviations

E_g : Conduction band; EELS: Electron energy loss spectroscopy; E_F : Fermi level; FTO: F:SnO₂; HR-TEM: High-resolution transmission electron microscopy; IPCE: Incident photon-to-current efficiency; J-V: Photocurrent density–potential; M-S: Mott-Schottky; N_d : Donor density; NRs: Nanorods; NTs: Nanotubes; PEC: Photoelectrochemical; PID: Proportional–integral–derivative; RTA: Rapid thermal annealing; SEM: Scanning electron microscopy; V_{fb} : Flat band potential; XRD: X-ray diffraction

Acknowledgements

We would like to thank Prof. G. Garnweitner for Autoclave support from Institut für Partikeltechnik and M. Karsten, W. Weiß, K.-H. Lachmund, A. Schmidt and J. Arens for technical assistance. We thank Z. Pei and Prof. C. Zhi from Department of Physics and Materials Science, City University of Hong Kong for the support of IPCE measurement.

Funding

This work was mainly supported by the institute fundings of Institute for Semiconductor Technology, TU Braunschweig and Fraunhofer Institute for Surface Engineering and Thin Films. X.Wang acknowledges the support by scholarship from the China Scholarship Council (CSC) under the Grand CSC No. 201206950015. This work was partially supported by General Research Fund (612113) from Hong Kong Research Grant Council, ITS/362/14FP from Hong Kong Innovation Technology Commission.

Authors' Contributions

XW and HS generated the research idea, analyzed the data, and wrote the paper. XW, SE, YL, FY, LL, and HZ carried out the experiments and the measurements. LS, GB, and AW supervised and discussed the whole work. ZF, SG, and FP participated in the discussions. All authors read and approved the final manuscript.

Competing Interests

The authors declare that they have no competing interests.

Publisher's Note

Springer Nature remains neutral with regard to jurisdictional claims in published maps and institutional affiliations.

Author details

¹Institute for Semiconductor Technology, TU Braunschweig, Hans-Sommer-Strasse 66, 38106 Braunschweig, Germany. ²Laboratory for Emerging Nanometrology (LENA), TU Braunschweig, Langer Kamp 6, 38106 Braunschweig, Germany. ³Department d'Electrònica, Universitat de Barcelona, c/Martí Franquès 1, 08028 Barcelona, Spain. ⁴Department of Electronic and Computer Engineering, The Hong Kong University of Science and Technology, Clear Water Bay, Kowloon, Hong Kong, SAR, China. ⁵Fraunhofer Institute for Surface Engineering and Thin Films, Bienroder Weg 54E, 38108 Braunschweig, Germany. ⁶School of Chemistry and Chemical Engineering, Jiangsu University, Xuefu Road 301, 212013 Zhenjiang, China.

Received: 28 February 2017 Accepted: 22 April 2017

Published online: 05 May 2017

References

- Chen X, Liu L, Yu PY, Mao SS (2011) Increasing solar absorption for photocatalysis with black hydrogenated titanium dioxide nanocrystals. *Science* 331:746–750
- Wang Z, Yang C, Lin T, Yin H, Chen P, Wan D, Xu F, Huang F, Lin J, Xie X, Jiang M (2014) H-doped black titania with very high solar absorption and excellent photocatalysis enhanced by localized surface plasmon resonance. *Adv Funct Mater* 23:5444–5450
- Liu L, Chen X (2014) Titanium dioxide nanomaterials: self-structural modifications. *Chem Rev* 114:9890–9918, and references within
- Wang G, Wang H, Ling Y, Tang Y, Yang X, Fitzmorris RC, Wang C, Zhang JZ, Li Y (2011) Hydrogen-treated TiO₂ nanowire arrays for photoelectrochemical water splitting. *Nano Lett* 11:3026–3033
- Liu N, Schneider C, Freitag D, Hartmann M, Venkatesan U, Müller J, Spiecker E, Schmuki P (2014) Black TiO₂ nanotubes: cocatalyst-free open-circuit hydrogen generation. *Nano Lett* 14:3309–3313
- Kapadia R, Fan Z, Takei K, Javey A (2012) Nanopillar photovoltaics: materials, processes, and devices. *Nano Energy* 1:132–144
- Kapadia R, Fan Z, Javey A (2010) Design constraints and guidelines for CdS/CdTe nanopillar based photovoltaics. *Appl Phys Lett* 96:103116–1
- Leung SF, Zhang Q, Xiu F, Yu D, Ho JC, Li D, Fan Z (2014) Light management with nanostructures for optoelectronic devices. *J Phys Chem Lett* 5:1479–1495
- Mo LB, Bai Y, Xiang QY, Li Q, Wang JO, Ibrahim K, Cao JL (2014) Band gap engineering of TiO₂ through hydrogenation. *Appl Phys Lett* 105:202114–1
- Hill C, Jones S, Boys D (1989) Rapid thermal annealing—theory and practice. In: Levy RA (ed) *Reduced thermal processing for ULSI*. Springer, US, pp 143–180
- Xu SJ, Wang XC, Chua SJ, Wang CH, Fan WJ, Jiang J, Xie XG (1998) Effects of rapid thermal annealing on structure and luminescence of self-assembled InAs/GaAs quantum dots. *Appl Phys Lett* 72:3335–3337
- Feng X, Shankar K, Varghese OK, Paulose M, Latempa TJ, Grimes CA (2008) Vertically aligned single crystal TiO₂ nanowire arrays grown directly on transparent conducting oxide coated glass: synthesis details and applications. *Nano Lett* 8:3781–3786
- Liu B, Aydil ES (2009) Growth of oriented single-crystalline rutile TiO₂ nanorods on transparent conducting substrates for dye-sensitized solar cells. *J Am Chem Soc* 131:3985–3990
- Li J, Hoffmann MWG, Shen H, Fabrega C, Prades JD, Andreu T, Hernandez-Ramirez F, Mathur S (2012) Enhanced photoelectrochemical activity of an excitonic staircase in CdS@TiO₂ and CdS@anatase@rutile TiO₂ heterostructures. *J Mater Chem* 22:20472–20476
- Xie S, Li M, Wei W, Zhai T, Fang P, Qiu R, Lu X, Tong Y (2014) Gold nanoparticles inducing surface disorders of titanium dioxide photoanode for efficient water splitting. *Nano Energy* 10:313–321
- Liu L, Yu PY, Chen X, Mao SS, Shen DZ (2013) Hydrogenation and disorder in engineered black TiO₂. *Phys Rev Lett* 111:065505–1
- Fàbrega C, Monllor-Satoca D, Ampudia S, Parra A, Andreu T, Morante JR (2013) Tuning the fermi level and the kinetics of surface states of TiO₂ nanorods by means of ammonia treatments. *J Phys Chem C* 117:20517–20524
- Qiu Y, Leung SF, Zhang Q, Hua B, Lin Q, Wei Z, Tsui KH, Zhang Y, Yang S, Fan Z (2014) Efficient photoelectrochemical water splitting with ultrathin films of hematite on three-dimensional nanophotonic structures. *Nano Lett* 14:2123–2129
- Qiu Y, Leung SF, Wei Z, Lin Q, Zheng X, Zhang Y, Fan Z, Yang S (2014) Enhanced charge collection for splitting of water enabled by an engineered three-dimensional nanospire array. *J Phys Chem C* 118:22465–22472
- Lu H, Deng K, Yan N, Ma Y, Gu B, Wang Y, Li L (2016) Efficient perovskite solar cells based on novel three-dimensional TiO₂ network architectures. *Sci Bull* 61:778–786
- Caccamo L, Hartmann J, Fabrega C, Estrade S, Lilienkamp G, Prades JD, Hoffmann MWG, Ledig J, Wagner A, Wang X, Lopez-Conesa L, Peiro F, Reblad JM, Wehmann HH, Daum W, Shen H, Waag A (2014) Band engineered epitaxial 3D GaN-InGaN core-shell rod arrays as an advanced photoanode for visible-light-driven water splitting. *ACS Appl Mater Interfaces* 6:2235–2240
- Cho IS, Chen Z, Forman AJ, Kim DR, Rao PM, Jaramillo TF, Zheng X (2011) Branched TiO₂ nanorods for photoelectrochemical hydrogen production. *Nano Lett* 11:4978–4984
- Cho IS, Lee CH, Feng Y, Logar M, Rao PM, Cai L, Kim DR, Sinclair R, Zheng X (2013) Codoping titanium dioxide nanowires with tungsten and carbon for enhanced photoelectrochemical performance. *Nat Commun* 4:1723–1
- Lü X, Chen A, Luo Y, Lu P, Dai Y, Enriquez E, Dowden P, Xu H, Kotula PG, Azad AK (2016) Conducting interface in oxide homojunction: understanding of superior properties in black TiO₂. *Nano Lett* 16:5751–5755
- Yang C, Wang Z, Lin T, Yin H, Lü X, Wan D, Xu T, Zheng C, Lin J, Huang F, Xie X, Jiang M (2013) Core-shell nanostructured “black” rutile titania as excellent catalyst for hydrogen production enhanced by sulfur doping. *J Am Chem Soc* 135:17831–17838
- Pesci FM, Wang G, Klug DR, Li Y, Cowan AJ (2013) Efficient suppression of electron-hole recombination in oxygen-deficient hydrogen-treated TiO₂ nanowires for photoelectrochemical water splitting. *J Phys Chem C* 117: 25837–25844
- Yan P, Liu G, Ding C, Han H, Shi J, Gan Y, Li C (2015) Photoelectrochemical water splitting promoted with a disordered surface layer created by electrochemical reduction. *ACS Appl Mater Interfaces* 7:3791–3796
- Yang Y, Ling Y, Wang G, Liu T, Wang F, Zhai T, Tong Y, Li Y (2015) Photohole induced corrosion of titanium dioxide: mechanism and solutions. *Nano Lett* 15:7051–7057
- Leshuk T, Parviz R, Everett P, Krishnakumar H, Varin RA, Gu F (2013) Photocatalytic activity of hydrogenated TiO₂. *ACS Appl Mater Interfaces* 5:1892–1895